

Article

Austenite Reverse Transformation in a Q&P Route of Mn and Ni Added Steels

Maribel Arribas ^{1,*}, Teresa Gutiérrez ¹, Eider Del Molino ^{1,2}, Artem Arlazarov ³, Irene De Diego-Calderón ³, David Martin ⁴, Daniele De Caro ⁵, Sudhindra Ayenampudi ⁶ and Maria J. Santofimia ⁶

¹ Tecnalia, Basque Research and Technology Alliance (BRTA), Parque Científico y Tecnológico de Bizkaia, Astondo Bidea, 700, E-48160 Derio, Spain; teresa.gutierrez@tecnalia.com (T.G.); eider.delmolino@tecnalia.com (E.D.M.)

² Department Mining, Metallurgical and Materials Science, UPV/EHU, Plaza Torres Quevedo 1, 48013 Bilbao, Spain

³ ArcelorMittal Maizieres Research SA, Voie Romaine-BP30320, 57283 Maizières-lès-Metz, France; artem.arlazarov@arcelormittal.com (A.A.); irene.dediegocalderon@arcelormittal.com (I.D.D.-C.)

⁴ Swerim AB, Box 7047 SE-164 07 Kista, Sweden; david.martin@Swerim.se

⁵ Centro Ricerche Fiat, Corso Settembrini 40, Porta 8, Corpo 1, 10135 Torino, Italy; daniele.de-caro@fcagroup.com

⁶ Department of Materials Science and Engineering, Delft University of Technology, Mekelweg 2, 2628 CD Delft, The Netherlands; S.Ayenampudi@tudelft.nl (S.A.); M.J.SantofimiaNavarro@tudelft.nl (M.J.S.)

* Correspondence: maribel.arribas@tecnalia.com; Tel.: +34-667178882

Received: 29 May 2020; Accepted: 22 June 2020; Published: 29 June 2020

Abstract: In this work, four low carbon steels with different contents of Mn and Ni were heat treated by quenching and partitioning (Q&P) cycles where high partitioning temperatures, in the range of 550 °C–650 °C, were applied. In order to elucidate the effect of applying these high partitioning temperatures with respect to more common Q&P cycles, the materials were also heat treated considering a partitioning temperature of 400 °C. The microstructure evolution during the Q&P cycles was studied by means of dilatometry tests. The microstructural characterization of the treated materials revealed that austenite retention strongly depended on the alloy content and partitioning conditions. It was shown that the occurrence of austenite reverse transformation (ART) in the partitioning stage in some of the alloys and conditions was a very effective mechanism to increase the austenite content in the final microstructure. However, the enhancement of tensile properties achieved by the application of high partitioning temperature cycles was not significant.

Keywords: quenching and partitioning; austenite reverse transformation; Mn and Ni influence; austenite stabilization

1. Introduction

Quenching and partitioning (Q&P) steels have been demonstrated to provide outstanding mechanical properties due to the novel microstructure formed mainly by martensite and retained austenite [1–4]. These properties make Q&P steels very attractive for the automotive sector. In the Q&P process, the steel is first quenched to a predetermined temperature (quench temperature, QT) in the M_s – M_f (i.e., martensite start and finish temperatures) temperature range to produce a partially martensitic and partially austenitic microstructure. Second, in the so-called partitioning step, carbon is partitioned from carbon enriched martensite into austenite due to the difference in carbon chemical

potential. Thus, carbon stabilized austenite is retained in the microstructure after a final quenching to room temperature [5]. Depending on the alloy composition and Q&P conditions, competitive reactions can also occur in the partitioning stage such as austenite decomposition into bainite [6] and carbide formation inside primary martensite [7], which reduces the fraction of austenite in the microstructure and the carbon available for partitioning, respectively.

The high retained austenite fractions present in Q&P steels are believed to result in an improved strength and ductility balance [1,8]. Consequently, most research studies are focused on increasing the final fraction of retained austenite (RA), mainly by optimizing the process conditions and chemical composition of the alloys. Since carbon is an interstitial alloying element, partitioning temperatures equal and lower than 450 °C have been shown to be sufficient for an effective carbon partitioning at relatively short times of typically less than a few minutes. However, the application of high partitioning temperatures has the potential to lead to microstructures with even higher fractions of retained austenite. This assessment is based on two different mechanisms.

- a) First, diffusion of substitutional alloying elements such as Mn and Ni is expected to increase in the higher temperature range and can further stabilize austenite in a Q&P route. This idea is supported by the work of some authors [9,10], who have shown via atom probe tomography (APT) that in the Q&P route, apart from carbon, the partitioning of other alloying elements such as Mn occurs in some of the martensite/austenite interfaces at 400 °C. Seo et al. [11] provided direct atomic-scale evidence for the partitioning of both interstitial carbon and substitutional Mn and Si during the Q&P processing of medium Mn steel with a partitioning temperature of 450 °C. However, Ayanampudi et al. [12] also applied high partitioning temperatures (PT) in the 400 °C–600 °C range to a medium Mn steel, and observed that high partitioning temperatures promoted cementite precipitation in austenite films and pearlite formation in blocky austenite, resulting in a decrease in the fraction of retained austenite with holding time. They concluded that the successful application of high temperature partitioning treatments requires microstructure design strategies to minimize or suppress competitive reactions.
- b) Second, high partitioning temperatures may lead to austenite reverse transformation (ART), which can also be explored as a mechanism to increase the final content of retained austenite. ART taking place in the intercritical annealing of medium Mn steels has been proven to provide a high amount of austenite in the final microstructure [13–15]. The key process is to heat the steel with an original martensitic microstructure to the intercritical region where part of the martensite is reverted to austenite. During annealing, diffusion of both carbon and manganese occurs, which determines both the phase fraction and stability of the retained austenite. The occurrence of ART in Q&P heat treatments was previously analyzed by Ding et al. [16], who reported the formation of new austenite by reheating the initial primary martensite + pre-existing austenite microstructure to the intercritical region in a Fe-0.2C-8Mn-2Al steel alloy. The austenite formed during the partitioning stage was enriched with Mn and hence, during the final quench, reverted austenite was more stable than pre-existing austenite.

In the present work, Q&P thermal cycles with high partitioning temperatures were investigated. In the proposed high PT process, the first quenching step was similar to conventional treatments. However, the partitioning stage was done at temperatures higher than those in the conventional in the 550 °C to 650 °C range, and the results were compared with those obtained after partitioning at 400 °C. The occurrence of ART during the partitioning was investigated. Additionally, the influence of different Mn and Ni contents in this new route that comprises ART in Q&P heat treatments was explored. The present work contributes to the understanding of the effectiveness of high partitioning temperature Q&P cycles in retaining a high amount of austenite in the final microstructure as well as studying the resulting mechanical properties and analyzing the effect of Mn and Ni contents, which have not been addressed in previous studies.

2. Materials and Methods

Ingots of four steel grades with different contents of Mn and Ni were produced in the laboratory using a vacuum induction melting furnace. The chemical composition of the four steel grades is

shown in Table 1 and referred to as 2Mn, 4Mn, 6Mn, and 6Mn2Ni. The ingots were reheated to ~1250 °C and a roughing stage was performed to decrease the thickness from 60 mm to 30 mm. The obtained slabs were then cut into five small ingots that were reheated to ~1250 °C and hot rolled. The hot rolling consisted of five hot rolling passes (T_{end} of rolling approximately above 900 °C) and coiling at 500 °C. The softening annealing consisted of isothermal holding at 600 °C for 1 h followed by water quenching. Finally, samples were cold rolled to 1.5 mm thick sheets. Hot rolled materials were characterized before and after softening annealing by microstructure observation with a light optical microscope (LOM) after polishing up to 1 μm and etching with sodium metabisulfite. Vickers microhardness tests with 9.8 N load were also performed with the hot rolled samples.

Table 1. Chemical composition of the steels (wt.%).

| Steel | C | Mn | Ni | Si | P | S | N |
|--------|------|-----|-----|-----|-------|--------|--------|
| 2Mn | 0.20 | 2.0 | 0.0 | 1.5 | 0.013 | 0.0015 | 0.0031 |
| 4Mn | 0.19 | 3.8 | 0.0 | 1.4 | 0.012 | 0.0017 | 0.0035 |
| 6Mn | 0.19 | 5.8 | 0.0 | 1.4 | 0.011 | 0.0013 | 0.0033 |
| 6Mn2Ni | 0.19 | 5.7 | 1.6 | 1.4 | 0.014 | 0.0019 | 0.0041 |

The Q&P cycle simulations were performed using a Gleeble 3800 system fitted with a large sample sheet annealing rig and employed specimens that were 250 mm in length and 50 mm in width. Figure 1 shows the details of the Q&P thermal cycle. The samples were heated to a temperature of $A_{c3} + 50$ °C and isothermally held for 120 s. The heat treatment was followed by interrupted quenching at 100 °C/s in the 2Mn alloy and 20 °C/s in the other alloys. The quenching temperature was established to achieve a volume fraction of austenite equal to 0.25 (QT25). The samples were held at this temperature for 5 s and then heated up at 10 °C/s to different partitioning temperatures. Three high partitioning temperatures of 550 °C, 600 °C, and 650 °C, and a partitioning time (Pt) of 500 s were selected. Additionally, a conventional PT of 400 °C with a holding time of 300 s was applied. The latter was considered as a reference condition to better assess the influence of high partitioning temperature cycles. The final cooling to room temperature was done at 50 °C/s. Afterward, the Gleeble samples were machined for further microstructure and mechanical characterization, taking samples from a central area.

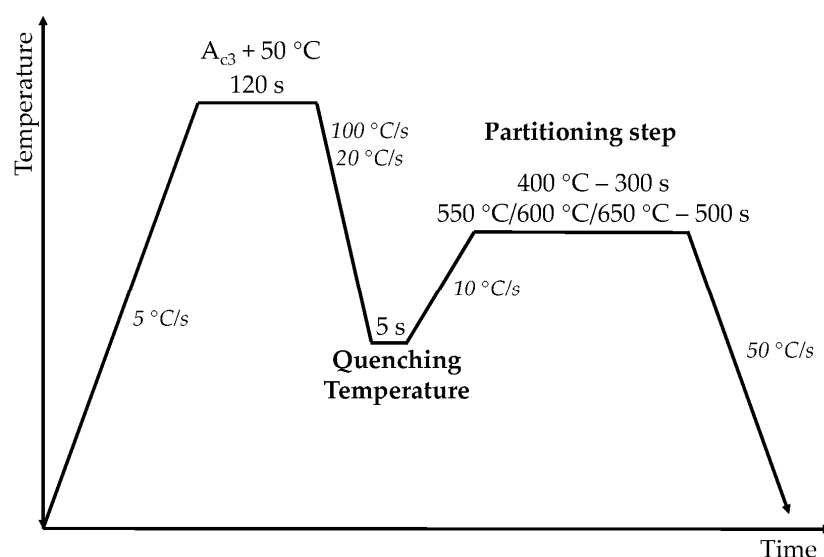


Figure 1. Scheme of the quenching and partitioning (Q&P) processing cycle applied in both the Gleeble system and dilatometer.

Phase transformation temperatures A_{c1} , A_{c3} , and M_s , which are critical cooling rates needed to avoid diffusion-based phase transformations (CCR) and QT25 temperatures, were obtained by means of a LINSEIS L78 RITA dilatometer using cylindrical samples with a 3 mm diameter and 10 mm

length. Resulting values are reported in Table 2. First, A_{c1} and A_{c3} temperatures were determined by heating the samples at 5 °C/s up to 1000 °C. Then, M_s , CCR, and QT25 were determined by considering an austenization temperature equal to $A_{c3} + 50$ °C and a holding of 120 s. Critical cooling rates were measured by analyzing the different cooling rates for each alloy. In order to determine M_s and QT25 temperatures, samples were cooled down to room temperature by employing a cooling rate above CCR, specifically at 100 °C/s for alloy 2Mn and at 20 °C/s in the others, and then were reheated up to 500 °C at 5 °C/s. From the resulting dilatometry curves, applying the lever rule between the expansion of the untransformed austenite curve and that from the reheating, martensite transformation curves were calculated. Thus, quenching temperatures that corresponded to 0.25 of untransformed austenite were determined.

Table 2. Experimental phase transformation temperatures, critical cooling rate (CCR) to avoid diffusion-based phase transformations, quenching temperature where 0.25 austenite exists (QT25), and temperature for the start of austenite reverse transformation (ART T_{start}) in the studied steels considering an austenization temperature of $A_{c3} + 50$ °C.

| Steel | A_{c1} (°C) | A_{c3} (°C) | M_s (°C) | CCR (°C/s) | QT25 (°C) | ART T_{start} (°C) |
|--------|---------------|---------------|------------|------------|-----------|----------------------|
| 2Mn | 760 | 870 | 365 | 60 | 300 | 708 |
| 4Mn | 730 | 830 | 310 | 0.5–2 | 240 | 680 |
| 6Mn | 695 | 790 | 240 | < 0.1 | 145 | 660 |
| 6Mn2Ni | 690 | 790 | 220 | < 0.1 | 120 | 640 |

The Q&P cycles shown in Figure 1 were also applied in the dilatometer in order to analyze the microstructure evolution in the different alloys during the respective heat treatments. Additionally, the start of austenite reverse transformation in the heating from QT was determined by dilatometry tests. For this, samples were heated at $A_{c3} + 50$ °C, held for 120 s, cooled down as previously described until QT25, and afterward, the samples were re-heated up to $A_{c3} + 50$ °C at 10 °C/s. The temperature at which the austenite reverse transformation started was determined from the volume contraction observed in the dilatometry curve and is shown in Table 2.

The fractions of the retained austenite in the Q&P processed Gleeble samples were obtained by x-ray diffraction (XRD). Steel samples of 10 × 10 mm² were mechanically ground to a quarter thickness and polished down to 1 μm to obtain a mirror surface. Then, the surface was additionally electropolished to take out the mechanical effects of preparation. X-ray diffraction measurements were done using a BRUKER D8 Discover diffractometer with a cobalt tube (Co $K\alpha$ radiation with $\lambda = 1.8$ Å) under 35 kV and 40 mA. Scans were acquired in the θ -2 θ configuration. In order to avoid the influence of texture, samples were continuously rotated during measurement with the following angle variations: ψ from 0° to 60° with a step of 5° and φ from 0° to 360°. The spectra were analyzed using the commercial TOPAS software and applying the Rietveld refinement method. RA fractions were evaluated using the (200), (211), and (220) peak spectra.

The microstructures of the selected Q&P treated Gleeble samples were observed with a Schottky field emission gun scanning electron microscope (FEGSEM) (JEOL JSM-7000F) after conventional metallography preparation, polishing up to 1 μm, and etching with Nital 2%. Electron backscatter diffraction (EBSD) scans were performed on selected samples and prepared using similar metallographic techniques, followed by a final polishing with OP-U (colloidal silica) for 15 minutes. The acquisition of EBSD scans was done using a step size of 30 nm.

Finally, room-temperature tensile tests were performed on Q&P treated samples by employing a standard geometry of 50 mm gauge length. A universal INSTRON tensile testing machine was employed with a strain rate of 0.001 s⁻¹ and equipped with a contact extensometer.

3. Results and Discussion

3.1. Base Material Characterization

The results of the hardness measurements of hot rolled materials at different steps, together with some examples of the observed microstructures, are presented in Figure 2. The hardness of alloy 2Mn was 224 HV, which is acceptable for further cold rolling and therefore was not heat treated. In contrast, the obtained hardness of other alloys was quite high (370 HV–560 HV). This means that direct cold rolling of these hot rolled sheets was difficult, and therefore specific softening treatments were applied as explained in the previous section. After the softening treatments, the obtained hardness was in the range of 270 HV–360 HV, which allows for laboratory cold rolling procedures.

As can be seen in the micrographs shown in Figure 2, alloy 2Mn mainly presented a ferrite–pearlite structure with some minor fractions of bainite and martensite. The microstructure in the remaining alloys consisted of a mixture of bainite–martensite. In the case of alloy 4Mn, the major phase seemed to be bainite and in the alloys 6Mn and 6Mn2Ni, it was martensite. These microstructure observations were in agreement with the measured microhardness levels of the different hot rolled sheets. The presence of hard phases such as bainite and martensite was a consequence of the higher Mn and Ni contents added to the steels. Softening annealing performed on alloys 4Mn, 6Mn, and 6Mn2Ni resulted in the recovery of the structure (decrease of dislocation density), which was helpful in the reduction of steel hardness and, in some cases, led to the precipitation of carbides.

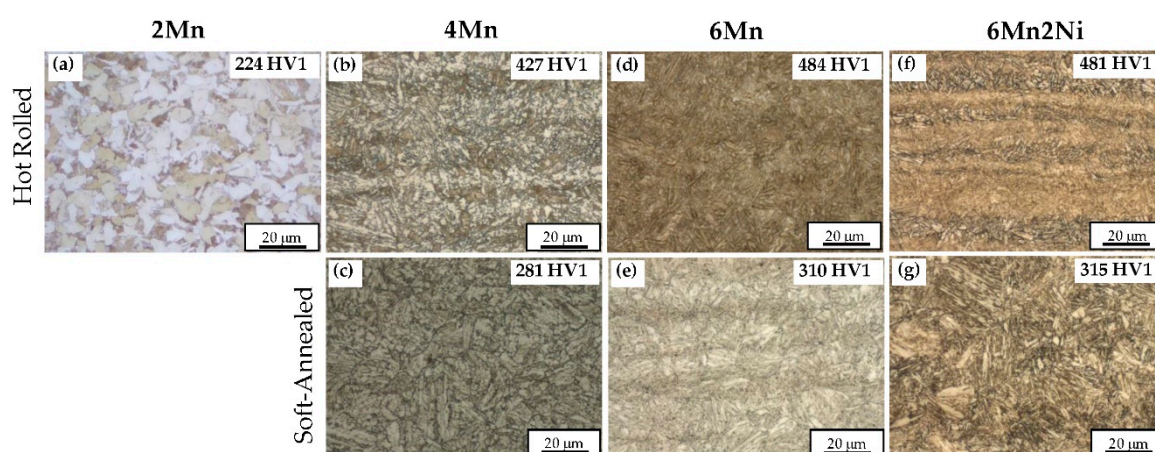


Figure 2. Light optical metallography (LOM) images and hardness of the hot strip microstructures. (a) Alloy 2 Mn after hot rolling; (b), (d), and (f) alloys 4Mn, 6Mn, and 6Mn2Ni after hot rolling, respectively; (c), (e), (g) alloys 4Mn, 6Mn, and 6Mn2Ni after soft annealing, respectively.

3.2. Microstructure Evolution during Quenching and Partitioning (Q&P) Heat Treatment

First, the final microstructures were characterized, and then, the results combined with dilatometry analysis allowed for the investigation of microstructure evolution at conventional and high PT cycles.

3.2.1. Characterization of Microstructure after Q&P Heat Treatment

Figure 3 presents the volume fraction of retained austenite measured by XRD for all the alloys and Q&P cycles. In the case of the 400 °C partitioning temperature cycle (PT400), the figure shows an increasing volume fraction of retained austenite with Mn, confirming the stabilization role of this element. Furthermore, the addition of 1.6 wt. % Ni in alloy 6Mn2Ni resulted in a further increase in the volume fraction of retained austenite in the final microstructure. However, the effect of Ni in austenite stabilization was comparatively less significant than the effect of Mn.

In the case of the 550 °C, 600 °C, and 650 °C partitioning temperature cycles (PT550, PT600, and PT650, respectively) in 2Mn and 4Mn alloys, the high partitioning temperature cycles were less effective in retaining austenite than the conventional partitioning done at 400 °C. In the 6Mn and 6Mn2Ni alloys, the results strongly depended on the PT condition. Thus, after partitioning at 550 °C, alloy 6Mn also presented a very low RA fraction, which was slightly raised by the addition of Ni. In

comparison, the PT600 cycle resulted in a higher RA volume fraction in both alloys. However, in both PT conditions, the obtained austenite contents were lower than after the PT400 cycle. The results drastically changed with the application of the PT650 cycle, obtaining final austenite contents much higher than those obtained with the PT400 cycle, which were specifically 0.34 and 0.44 in the 6Mn and 6Mn2Ni alloys, respectively.

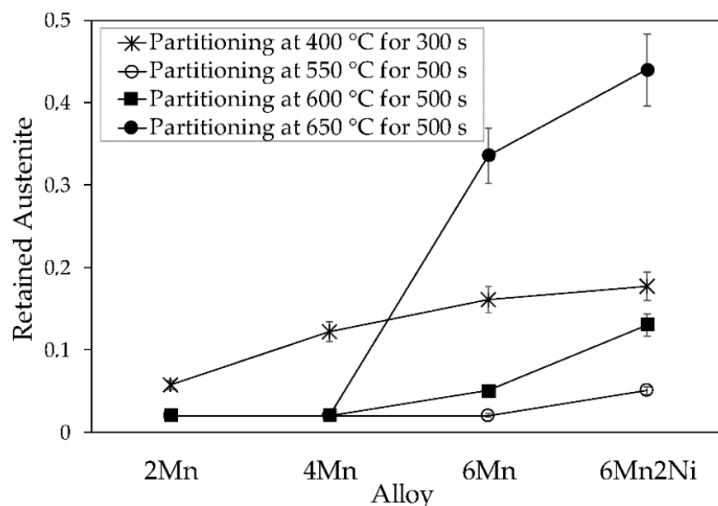


Figure 3. Retained austenite in the Q&P processed steels, partition-treated at conventional (400 °C) and high (550 °C, 600 °C, and 650 °C) partitioning temperatures.

Given the high RA fraction obtained in alloy 6Mn2Ni after the PT650 cycle, the final microstructure of this alloy was observed in the SEM. The microstructure of alloy 2Mn was also observed for comparison, since, in the same condition, it presented a very low RA fraction. The SEM micrographs are presented in Figure 4. In alloy 2Mn, the microstructure mainly consisted of tempered martensite containing carbides (Figure 4a). Carbides presented a coarse size and the start of pearlite formation could be appreciated in some regions. In alloy 6Mn2Ni, the distribution and morphology of the phases indicated a high amount of RA (Figure 4b). A bright thin lath type phase was observed, which was identified as retained austenite. The dark phase was identified as primary martensite (M1) where few carbides were observed and bigger islands with a smooth dark-grey aspect center and white edges were likely to be MA islands.

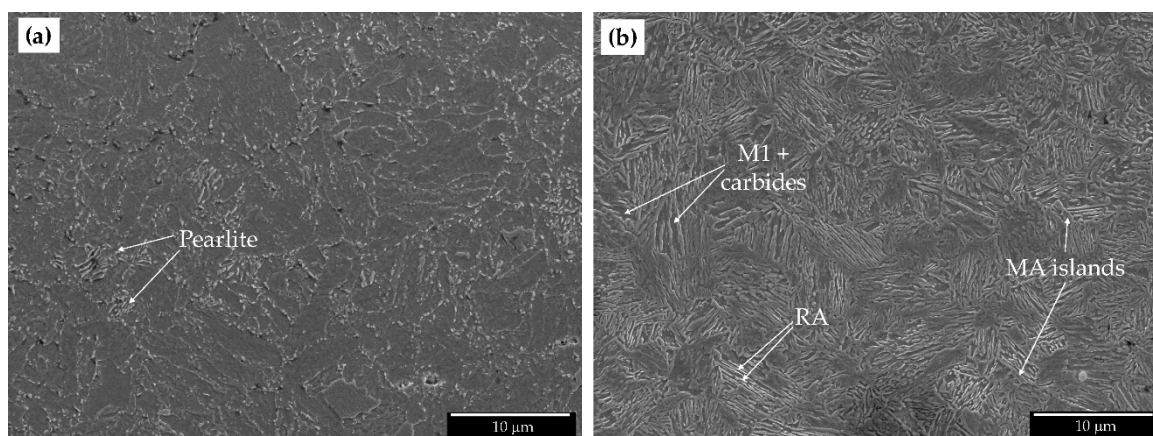


Figure 4. Field emission gun scanning electron microscopy (FEGSEM) micrograph of the Q&P processed alloys partition-treated at 650 °C for 500 s in alloys: (a) 2Mn and (b) 6Mn2Ni.

Additionally, EBSD phase maps were obtained in the 6Mn2Ni alloy partition-treated at 650 °C and 400 °C. EBSD images are shown in Figure 5, where the red phase was identified as RA, green

was martensite, and black indicates unidentified regions. As can be seen in Figure 5a, EBSD maps also revealed a high volume fraction of retained austenite in the PT650 condition. Specifically, the volume fraction of retained austenite determined by EBSD was 0.45, which was in very good agreement with the value measured by XRD. The fraction and distribution of the retained austenite grains clearly indicated austenite reverse transformation during the partitioning stage. In the low PT condition (Figure 5b), the volume fraction of RA determined by EBSD was 0.08, which was lower than the fraction measured by XRD. Austenite fractions determined by EBSD can be lower since the dark regions in the EBSD maps can be MA islands with retained austenite across the grain boundary. However, these regions are mostly recognized as unidentified regions. Additionally, the detection of nanometric film like retained austenite stabilized in between the martensitic laths is also difficult with EBSD.

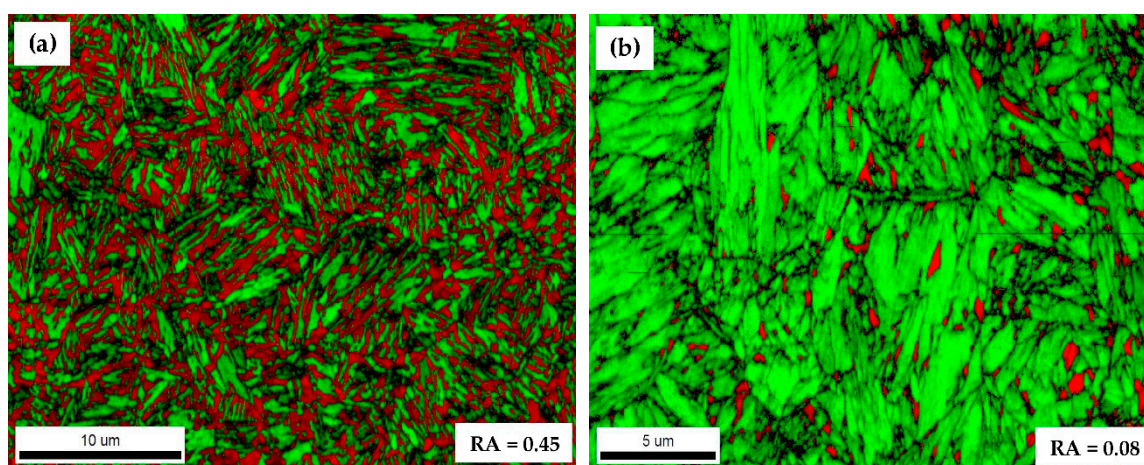


Figure 5. Electron backscatter diffraction (EBSD) phase maps showing retained austenite (RA) (red), primary martensite (green), and unidentified regions (black) in the 6Mn2Ni alloy partition-treated at (a) 650 °C for 500 s; (b) 400 °C for 300 s.

The volume fraction of phases existing after the application of Q&P treatments were estimated based on the dilatometry curves obtained in the simulation of Q&P cycles and the experimentally obtained RA results. Figure 6 presents the volume fraction of phases obtained for all the alloys and conditions considered. The volume fraction of phases were estimated according to the following procedure. The primary martensite fraction was equal to that present at QT, which was targeted to be 0.75. The slight variations in the primary martensite fraction that can be seen in Figure 6 are the consequence of considering the real QT achieved in the dilatometry experiments. Secondary martensite was obtained by comparing the change in length at the final cooling with the change in length given by the martensite transformation curve on the directly quenched sample. Retained austenite was experimentally measured by means of XRD measurements. Finally, the products formed by austenite decomposition in the partitioning stage were encompassed in the expression of “other phases”, which was calculated by phase fraction balance. In the conditions that ART occurred in the partitioning stage, RA and secondary martensite were obtained as described earlier, whereas primary martensite was calculated by balance. In this case, the reverted austenite fraction formed in the partitioning stage corresponded to the sum of retained austenite measured by XRD, plus the secondary martensite fraction, deducting the preliminary austenite fraction.

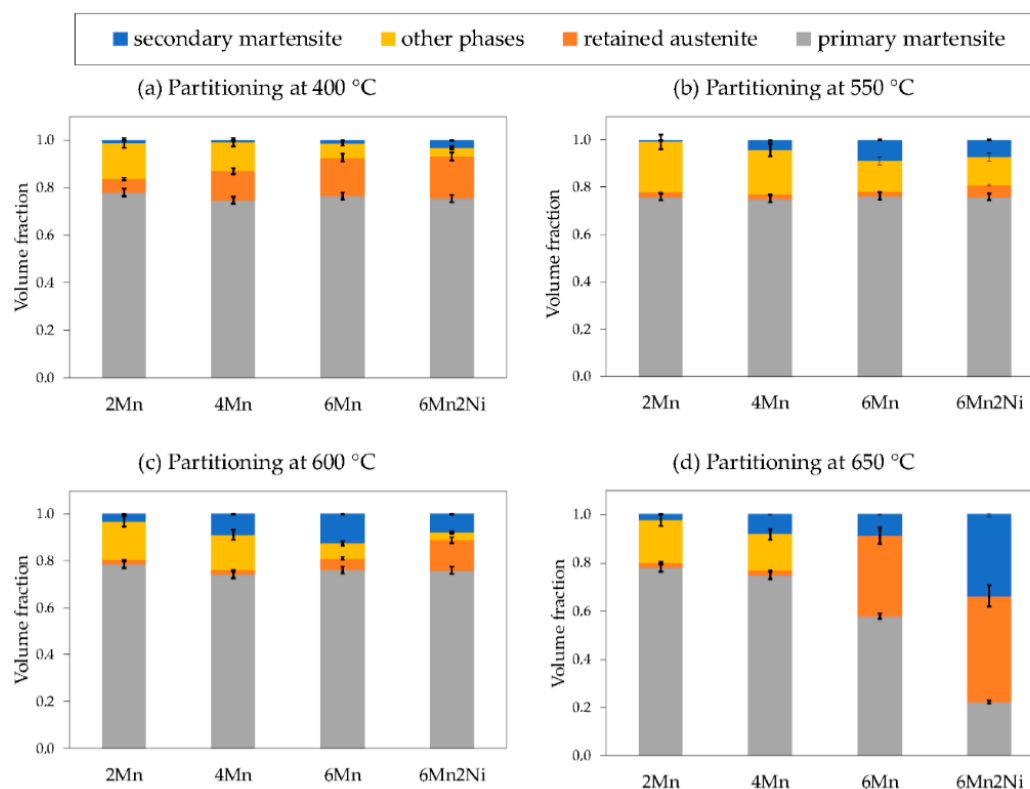


Figure 6. Volume fraction of phases after the application of (a) 400 °C; (b) 550 °C; (c) 600 °C; (d) 650 °C partitioning temperature cycles in alloys 2Mn, 4Mn, 6Mn, and 6Mn2Ni.

As can be seen in Figure 6, the volume fraction of austenite decomposition products was quite significant in many of the alloys and conditions. In order to aid in the analysis of the products formed in the partitioning stage, time-temperature-transformation (TTT) diagrams were obtained for each alloy using JMatPro-v9.1 software. Figure 7 presents the TTT diagrams calculated for an initial austenite grain size of 5 μm . Although not fully representative of the conditions existing at PT, these diagrams contributed to the understanding of the phenomenon occurring in the partitioning step. TTT diagrams showed that Mn addition shifted phase transformation curves to a lower temperature range and longer times. The addition of Ni mainly resulted in longer phase transformation times. The comparison between the TTT diagrams and experimental results is detailed in Section 3.2.2.

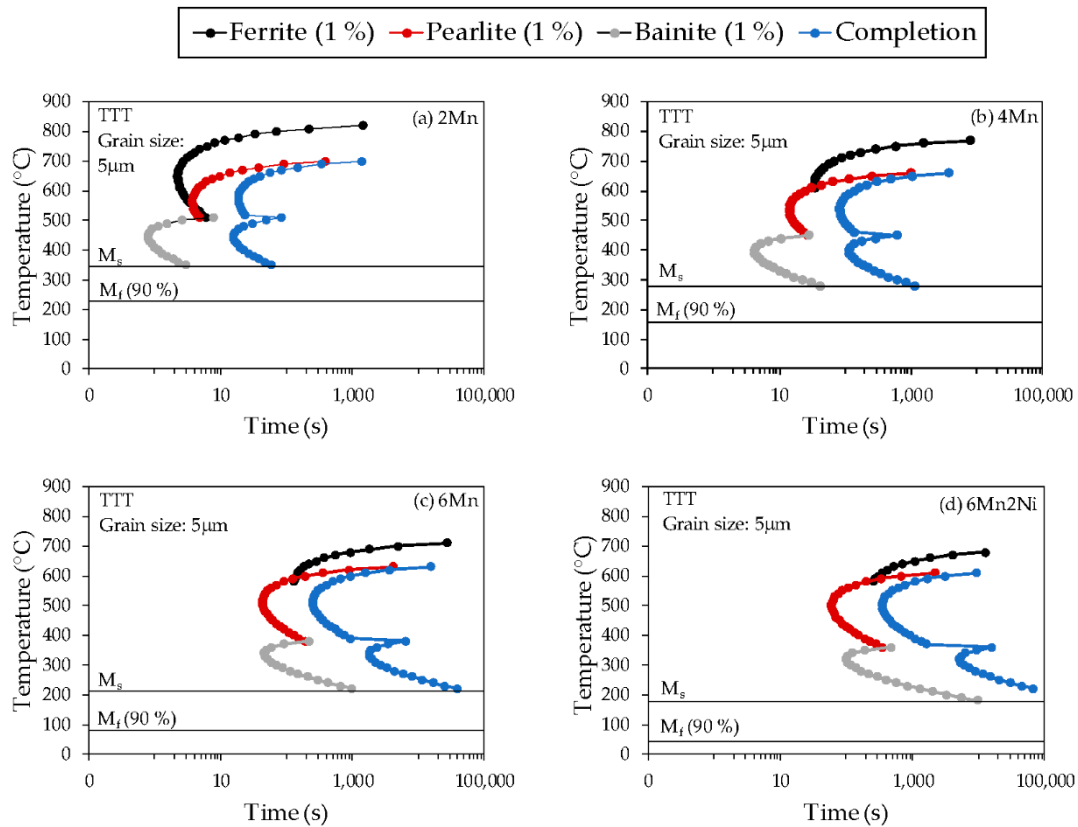


Figure 7. Time-temperature-transformation (TTT) diagrams calculated by JMatPro for an initial austenite grain size of 5 μm in alloys (a) 2Mn; (b) 4Mn; (c) 6Mn; (d) 6Mn2Ni.

3.2.2. Effect of Mn and Ni Alloying Elements on Microstructure Evolution

As mentioned earlier, the microstructure evolution during the Q&P cycle was discussed based on the dilatometry curves and volume fraction of phases determined in the final microstructure. Dilatometry curves obtained in the simulation of the different Q&P cycles are presented in Figure 8 for the four alloys. Dilatometry curves start at QT and represent the heating to PT, partitioning stage, and final cooling. The results obtained at the conventional partitioning condition of 400 °C and 300 s are discussed first for a later comparison with the behavior observed when the partitioning temperature was raised to the range of 550 °C to 650 °C.

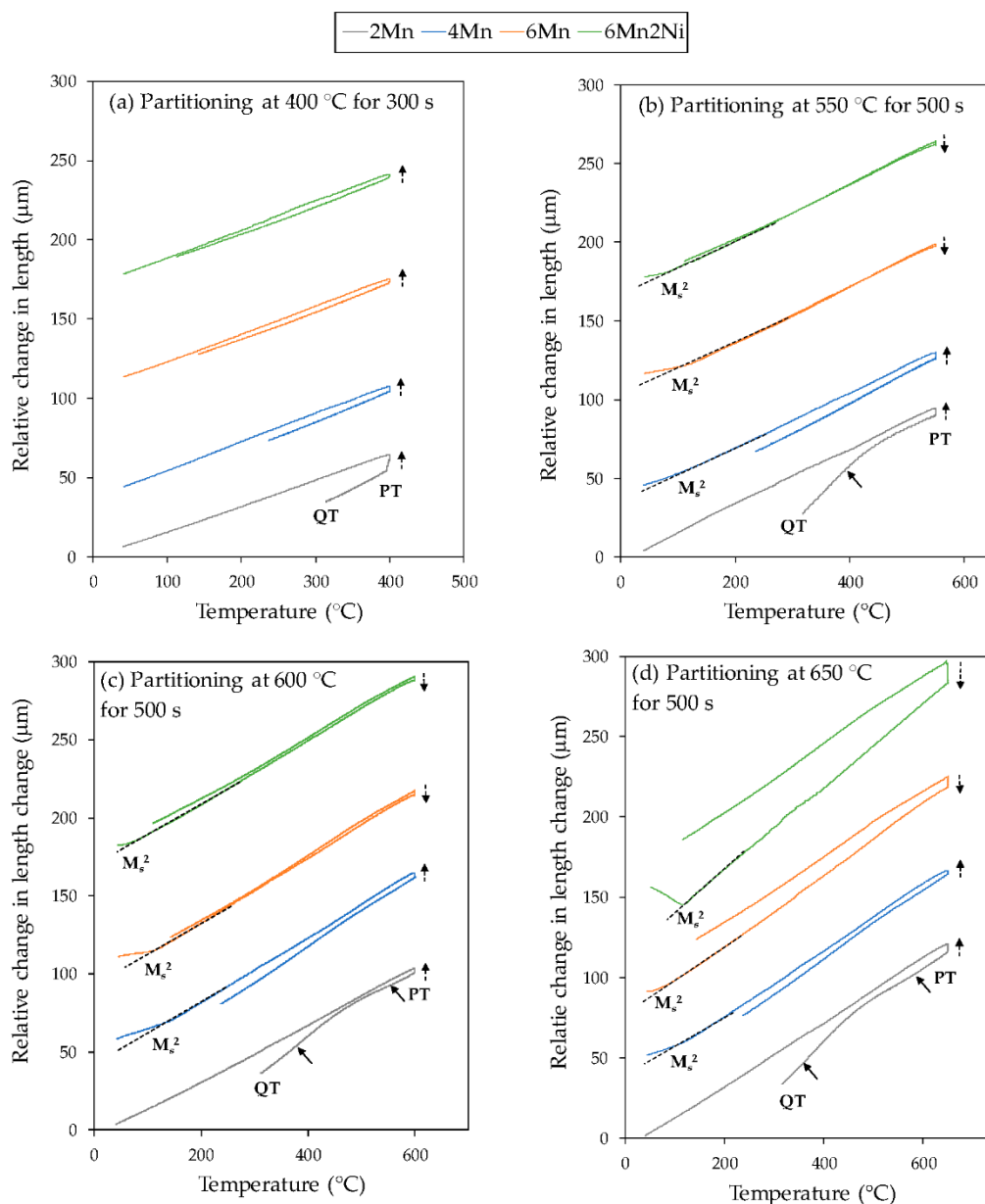


Figure 8. Dilatometry trace for the heating from quenching temperature (QT) to partitioning temperature (PT) in partition treatment at (a) 400 °C; (b) 550 °C; (c) 600 °C; (d) 650 °C and final quenching to room temperature. The start of secondary martensite formation in the final cooling is indicated by M_s^2 .

- Partitioning temperature – 400 °C

Dilatometry curves corresponding to the 400 °C partitioning temperature cycles are presented in Figure 8a for the four alloys. Continuous expansion was observed in the partitioning stage in the four alloys, as indicated in the figure by means of ascending discontinuous arrows. The measured expansion decreased as the alloying content increased. Considering the expansion as $\Delta L/L_0 \times 100$, where ΔL is the change in length of the specimen during the partitioning and L_0 is the initial length, 0.100%, 0.028%, 0.018%, and 0.017% values were obtained for the 2Mn, 4Mn, 6Mn, and 6Mn2Ni alloys, respectively. Santofimia et al. reported that volume expansion during the partitioning stage could be related with the decomposition of austenite to ferrite, bainite, or isothermal martensite transformation [6]. Carbon partitioning from supersaturated martensite to austenite can also cause volume expansion [12,17]. However, comparatively, austenite decomposition to bainite gives rise to a more pronounced expansion [6].

In the case of the lower alloyed 2Mn steel, the volume expansion was more evident and was likely to be related to austenite decomposition. However, in the 4Mn, 6Mn, and 6Mn2Ni alloys, it was not clear whether the observed volume expansion was only due to carbon partitioning or if austenite decomposition also contributed. According to the estimated volume fraction of phases (Figure 6a), the fraction of austenite decomposition products decreased with the addition of Mn and Ni. However, a significant fraction was obtained in alloys 4Mn, 6Mn, and 6Mn2Ni. Hence, it is likely that apart from carbon partitioning, austenite decomposition also contributed to the observed expansion in these alloys.

Possible austenite decomposition products were analyzed based on TTT diagrams (Figure 7). At 400 °C, austenite is predicted to decompose into bainite in alloys 2Mn and 4Mn and in pearlite in alloys 6Mn and 6Mn2Ni. However, the theoretical times for the start of pearlite phase transformation are significantly longer, which is in agreement with the lower fraction of austenite decomposition products estimated in alloys 6Mn and 6Mn2Ni.

Finally, the amount of secondary martensite formed in the four alloys was very low, obtaining the highest amount, the 0.03 volume fraction, in alloy 6Mn2Ni. As can be seen in the dilatometry curves, secondary martensite formation was not evident in the final cooling. This means that the austenite existing at the end of the partitioning stage was stable enough to be mostly untransformed upon final cooling.

- Partitioning temperature – 550 °C, 600 °C, 650 °C

In Figure 8b–d, the dilatometry curves are shown for partitioning temperatures of 550 °C, 600 °C, and 650 °C, respectively. Within the graphs, the discontinuous ascending or descending arrows indicate the expansive or contractive behavior of the samples during the partitioning stage. It can be seen that the results strongly depend on the alloying content. The lower Mn containing alloys, 2Mn and 4Mn, showed dilatation, whereas in the 6Mn and 6Mn2Ni alloys, continuous contraction was observed in all the cases.

Additionally, a volume change was observed in the final cooling in alloys 4Mn, 6Mn, and 6Mn2Ni, at the three high PTs, which denoted the formation of secondary martensite. This means that austenite, at the end of partitioning, was not stable enough to remain untransformed in the final cooling. In alloy 2Mn, this volume change was not detected, indicating that secondary martensite formation was not significant. Additionally, alloy 2Mn presented a non-linear dilatation during the heating from QT to PT, as can be observed in Figure 8b–d. For the remaining alloys, a linear expansion was registered during the heating. The non-linear expansion is likely to indicate the occurrence of a phase transformation in this alloy during the heating to PT. For the 550 °C partitioning temperature cycle, only the onset of the transformation was observed at around 393 °C. In the Q&P cycles with 600 °C and 650 °C as partitioning temperatures, the start and end of the transformation were estimated as 379 °C/552 °C and 358 °C/583 °C, respectively. These temperatures are marked with arrows in Figure 8b–d. Based on the previously presented SEM micrograph (Figure 4a), the observed expansion could be related with pearlite formation. Furthermore, since secondary martensite formation was not evident in the final cooling in the 2Mn alloy and the volume fraction of austenite was rather low in the final microstructure, it is likely that austenite was mostly decomposed during the heating to PT and holding at PT.

In the PT550 cycle, a higher Mn content did not result in more austenite in the final microstructure. According to the estimated volume fraction of phases (Figure 6b), the increase in Mn gave rise to a lower decomposition of austenite in the partitioning stage as the volume fraction of other phases diminished. However, the undecomposed austenite seemed to not be sufficiently stable and transformed into secondary martensite in the final cooling, resulting in a higher volume fraction of secondary martensite in the alloy with a higher Mn content. The addition of Ni in the 6Mn2Ni alloy seemed to be slightly favorable for austenite stabilization.

According to the TTT diagrams, isothermal holding at 550 °C decomposes austenite into pearlite in the four alloys. The formation of pearlite clearly reduces the carbon available for austenite stabilization. This is in agreement with the results found by Ayenampudi et al. [12], who found that strong competitive reactions such as pearlite formation occurred at 500 °C partitioning, decreasing

the final austenite content. However, pearlite formation would result in volume expansion [12], which was only observed in alloys 2Mn and 4Mn. In contrast, the 6Mn and 6Mn2Ni alloys gave rise to a slight contraction in the partitioning stage. Kannan et al. [18] and Onink et al. [19] showed that austenite films saturated with carbon tended to decompose into carbon-depleted austenite and cementite, and this phenomenon gave rise to contraction. Therefore, it seems that in alloys 2Mn and 4Mn, the main reaction leading to the decomposition of austenite in the partitioning was pearlite formation, and in 6Mn and 6Mn2Ni alloys, due to the higher Mn and Ni contents, pearlite formation was retarded and the main competitive reaction occurring during the partitioning was austenite decomposition into carbon depleted austenite and cementite. Both reactions resulted in a lower carbon available for austenite stabilization.

In the PT600 cycle, the volume fractions of phases were very similar in alloys 2Mn and 4Mn to those determined after the PT550 cycle (Figure 6b,c). The most significant difference was that lower fraction of other phases and an increase in the formation of secondary martensite were obtained in the PT600 cycle. This behavior denoted that the amount of austenite decomposed into pearlite was lower at 600 °C, which is in agreement with the theoretical TTT diagrams that place the nose of pearlite closer to 550 °C. However, the fraction of austenite was not stable enough and secondary martensite formed in the final cooling. The further addition of Mn and particularly Ni was more effective in retarding the competitive reactions occurring during the partitioning stage, which resulted in more retained austenite in the final microstructure. Nevertheless, at both 550 °C and at 600 °C, the occurrence of austenite decomposition reactions strongly competed with carbon partitioning as well as with the potential austenite stabilization by Mn and Ni, which is in agreement with the work published in [12].

In the PT650 cycle, the results of the volume fraction of phases were, as before, very similar in the 2Mn and 4Mn alloys (Figure 6d). However, partitioning at 650 °C on alloy 6Mn led to 0.34 retained austenite in the final microstructure. As described earlier, in this alloy and PT condition, volume contraction was observed in the partitioning stage. In this case, the high austenite volume fraction measured by XRD and EBSD and the distribution and morphology of austenite observed in the SEM and EBSD images pointed to the ART phenomenon as an explanation for the measured contraction.

The onset of ART was calculated by means of dilatometry tests, as described earlier. In Table 2, it can be seen that the ART phenomenon started at a temperature lower than the A_{c1} temperature determined in the first heating stage of the Q&P cycle. The difference between both temperatures was between 35 °C and 52 °C considering the four alloys and was related to the presence of pre-existing austenite, which likely reduced the nucleation step of the transformation.

The temperature for the start of ART was determined to be 660 °C in alloy 6Mn considering a continuous heating from QT. However, stopping the heating at 650 °C and keeping it there for 500 s resulted in the formation of a 0.19 volume fraction of reverted austenite. Thus, the austenite fraction at the end of the partitioning, which represented the accumulation of pre-existing austenite (0.24) and the reverted austenite contents, was 0.43. The latter volume fraction was below the equilibrium fraction at 650 °C predicted by ThermoCalc (v. 2018b), which was 0.55. Given that 0.09 of secondary martensite appeared in the final cooling, the finally retained austenite volume fraction was 0.34, which was considered a high volume fraction.

Therefore, an important finding in this work was that ART in Q&P routes can stabilize a high amount of austenite at room temperature in medium Mn steels. Additionally, it should be emphasized that, in comparison with the intercritical annealing of medium Mn steels, the treatment applied in the present work requires shorter partitioning times to stabilize a high amount of austenite. It is likely that the pre-existing austenite reduces the nucleation time for ART and overall results in lower annealing times needed for obtaining high austenite volume fractions. This finding can represent an important advantage in terms of industrialization.

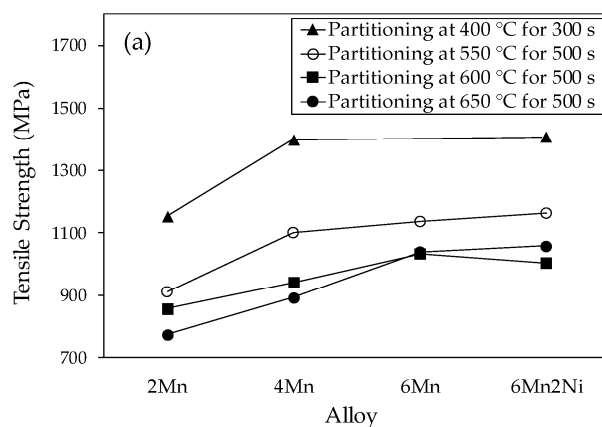
The occurrence of ART in Q&P heat treatments was previously analyzed by Ding et al. [16] in what they called the quenching-austenite reversion treatment. They reported the formation of new austenite by reheating the initial primary martensite + pre-existed austenite microstructure in the intercritical region in a Fe-0.2C-8Mn-2Al steel alloy. Considering a pre-existing austenite fraction of

0.20 and 0.30 and a partitioning done at 660 °C for one hour, the final RA measured by XRD was around 0.44 and 0.35, respectively. Here, for an initial austenite of 0.25, the final austenite was slightly lower at 0.34, which could be explained by the lower Mn addition in alloy 6Mn.

Finally, the addition of the 1.6 wt.% Ni in alloy 6Mn2Ni resulted in a further increase in the final fraction of austenite, obtaining a 0.44 volume fraction of RA after the application of the PT650 cycle. The addition of Ni resulted in a stronger contraction in the partitioning stage, as can be seen in Figure 8d. In this case, austenite formation in the continuous heating from QT was determined to start at 640 °C and the estimated austenite volume fraction at the end of the partitioning stage was 0.78, which corresponded to the pre-existing austenite (0.25) and new austenite formed in the partitioning (0.53). As this alloy presented a lower temperature for the start of ART, the driving force for austenite reversion was higher, which resulted in a very high austenite volume fraction. This value was indeed higher than the equilibrium fraction predicted by ThermoCalc at 650 °C, 0.70, which was likely due to the error in the estimation of the austenite fraction at the end of the partitioning, which was assumed to be 12%. Nevertheless, both numbers were of the same order and it can be said that the volume fraction at the end of the partitioning was very close to the equilibrium fraction predicted for alloy 6Mn2Ni. In alloy 6Mn2Ni, a very significant amount of secondary martensite, 0.34, was formed in the final cooling.

3.3. Tensile Properties

Tensile tests were performed in all the Q&P conditions and alloys. Tensile strength results are shown in Figure 9a and total elongation results in Figure 9b. It can be seen that in the conventional Q&P cycle with a partitioning temperature of 400 °C, the increase in Mn was beneficial for the tensile strength, however, it resulted in a noticeable decrease in elongation. A further increase in Ni content in alloy 6Mn2Ni did not modify tensile strength significantly and elongation was strongly reduced. The previously described characterization of the final microstructure indicated that retained austenite content increased by Mn and Ni additions. However, in the present case, the existence of a higher amount of austenite phase in the final microstructure did not result in better tensile properties. It seems like the main mechanism determining the tensile properties was the solid solution strengthening of Mn and Ni, although the characteristics of the austenite phase may also play a role, which requires further investigation.



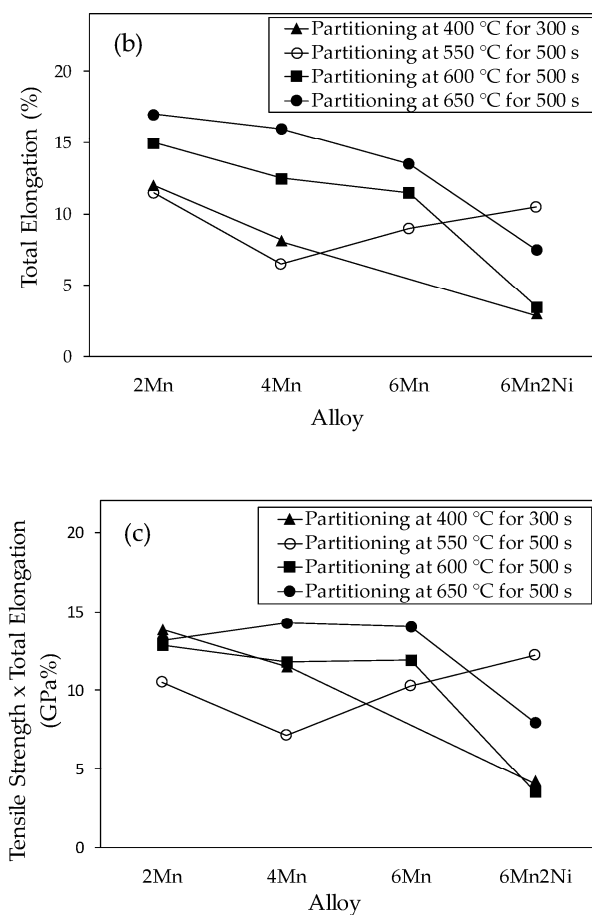


Figure 9. Tensile properties obtained in the Q&P processed steels, partition treated at 400 °C, 550 °C, 600 °C, and 650 °C representing: (a) tensile strength; (b) total elongation; (c) product of tensile strength and total elongation.

In comparison with the PT400 cycle, the higher PT cycles gave rise to a lower tensile strength, which was related to the tempering process of the martensite phase. In the high PT cycles, Mn additions were beneficial for strength and the influence of Ni was less noticeable, similar to the behavior observed after the PT400 cycle. Generally, elongation improves at higher partitioning temperature, which is mainly related with the tempering effect, and such a tendency was also confirmed in this work. Furthermore, it was shown that elongation decreased with Mn addition. It is worth highlighting the strong decrease in elongation caused by Ni additions at 600 °C and 650 °C and the clear improvement obtained at 550 °C. Similarly, the higher Mn in alloy 6Mn enhanced elongation at 550 °C with respect to alloy 4Mn, although it was still lower than in alloy 2Mn. The improvement of elongation obtained at 550 °C in alloys 6Mn and 6Mn2Ni with respect to 4Mn, but still below the value of 2Mn, should be further investigated.

The analysis of the product of tensile strength and total elongation (Figure 9c) did not reveal, generally, a significant improvement in the tensile properties by increasing the partitioning temperature. This was related to the fact that most of the treatments at 550 °C and 600 °C were not effective in stabilizing austenite due to the abundant competitive reactions. In the 650 °C PT cycles, alloy 6Mn2Ni gave rise to reverse austenite transformation and a 0.44 volume fraction of austenite was retained in the material. However, it did not provide the material with a high elongation (7.9% elongation). Alloy 6Mn partitioned at 650 °C also presented a high RA fraction in the final microstructure (0.34), however, elongation was not significantly improved (14%).

In this work, a clear relationship between the product of tensile strength and total elongation with volume fraction of retained austenite was not found, as can be seen in Figure 10. Alloy 6Mn was the only alloy where a direct relationship between both parameters was found, however, the

enhancement of tensile properties achieved at the highest RA fraction was similar to that found in alloys 2Mn and 4Mn with low fractions of RA. In alloy 6Mn2Ni, the product of tensile strength and total elongation found for the highest RA fraction was below the value obtained for the lowest RA fraction. Therefore, in this work, the addition of alloying elements like Mn and Ni and stabilizing higher fractions of RA did not result in improved mechanical properties.

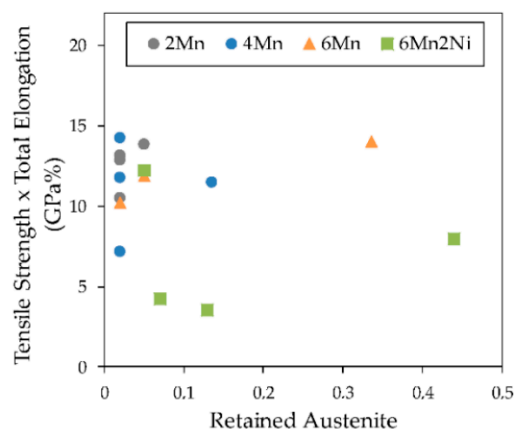


Figure 10. Relationship between the product of tensile strength and total elongation with retained austenite in the Q&P processed steels.

Ding et al. [16] observed that a small austenite fraction at QT (0.10) was beneficial for tensile strength and total elongation, however, preserving excessive austenite before ART (0.30 in their case) led to the formation of secondary martensite in the final microstructure, which makes the material very brittle. As shown before, the formation of secondary martensite in the final cooling was observed by dilatometry in the present work, which, in alloys 6Mn and 6Mn2Ni partitioned at 650 °C, might be the reason for the low elongation achieved despite the high amount of austenite. Based on the work published in [16], it is thought that a QT lower than QT25 employed in the present work could be beneficial for improving the mechanical properties in these alloys. Furthermore, the mechanical stability of RA may also play a role: in this work, it was suspected to be rather poor, however, more investigation is needed.

4. Conclusions

High partitioning temperature Q&P cycles were applied to four low carbon steels with different contents of Mn and Ni. In comparison with a conventional Q&P cycle with a partitioning temperature of 400 °C, the heat treatments with partitioning temperatures of 550 °C and 600 °C were less effective for stabilizing austenite in the final microstructure of the investigated steels. This was related with the occurrence of abundant competitive reactions: mainly pearlite formation and cementite precipitation. At these temperatures, a slight influence of Mn content on austenite stabilization was observed, with the effect of Ni more notable. However, the occurrence of ART at 650 °C permitted the stabilization of a high amount of austenite in the final microstructure, showing a clear influence of the Mn and Ni contents.

In general, the improvement of the tensile properties obtained by the application of high temperature cycles was not significant. In 550 °C and 600 °C partitioning cycles, it was related to the low stabilization of retained austenite due to the occurrence of abundant competitive reactions. At 650 °C, the high final austenite content did not result in better tensile properties, which might be due to the presence of a higher fraction of secondary martensite in the final microstructure, although a poor austenite mechanical stability may also play a role. It is understood that the addition of alloying elements like Mn and Ni and stabilizing higher fractions of RA does not necessarily enhance the mechanical properties of an alloy. Partitioning conditions play a key role in tailoring the mechanical properties of an alloy.

Author Contributions: Conceptualization, M.A., A.A., D.M., D.C., and M.J.S; Investigation, M.A., T.G., E.M., A.A., I.D.C, D.M., S.A., and M.J.S; Writing—original draft preparation, M.A.; Writing—review and editing, M.A., T.G., E.M., A.A., D.M., S.A., and M.J.S; Project administration, M.A. and T.G.; Funding acquisition, M.A., T.G., A.A., D.M., D.C., and M.J.S. All authors have read and agreed to the published version of the manuscript.

Funding: This research was carried out in the framework of the HIGHQP project, which has received funding from the Research Fund for Coal and Steel under grant agreement no. 709855. This study reflects only the author's views and the European Commission is not responsible for any use that may be made of the information contained therein.

Conflicts of Interest: The authors declare no conflicts of interest.

References

1. De Moor, E.; Lacroix, S.; Clarke, A.J.; Penning, J.; Speer, J.G. Effect of retained austenite stabilized via quench and partitioning on the strain hardening of martensitic steels. *Metall. Mater. Trans. A* **2008**, *39*, 2586–2595.
2. Arlazarov, A.; Ollat, M.; Masse, J.P.; Bouzat, M. Influence of partitioning on mechanical behavior of Q & P steels. *Mater. Sci. Eng. A* **2016**, *661*, 79–86.
3. Föjer, C.; Mahieu, J.; Bernier, N. Industrial production of quenching and partitioning steel. In *Proceedings of the International Symposium on New Developments in Advanced High-Strength Sheet Steels*, Vail, Colorado, 23–27 June 2013, AIST, USA, 2013.
4. Santofimia, M.; Nguyen-Minh, T.; Zhao, L.; Petrov, R.; Sabirov, I.; Sietsma, J. New low carbon Q & P steels containing film-like intercritical ferrite. *Mater. Sci. Eng. A* **2010**, *527*, 6429–6439.
5. Speer, J.; Matlock, D.K.; De Cooman, B.C.; Schroth, J.G. Carbon partitioning into austenite after martensite transformation. *Acta Mater.* **2003**, *51*, 2611–2622.
6. Santofimia, M.; Zhao, L.; Petrov, R.; Kwakernaak, C.; Sloof, W.G.; Sietsma, J. Microstructural development during the quenching and partitioning process in a newly designed low carbon steel. *Acta Mater.* **2011**, *59*, 6059–6068.
7. Mola, J.; De Cooman, B.C. Quenching and partitioning (Q & P) processing of martensitic stainless steels. *Metall. Mater. Trans. A* **2013**, *44*, 946–967.
8. De Moor, E.; Speer, J.G.; Matlock, D.; Penning, J.; Föjer, C. Effect of Si, Al and Mo alloying on tensile properties obtained by quenching and partitioning. In *Proceedings of Materials Science and Technology (MS & T)*, Pittsburg, PA, USA, 25–29 October 2009.
9. Santofimia, M.J.; Zhao, L.; Povstugar, I.; Choi P.P.; Raabe, D.; Sietsma, J. Carbon redistribution in a quenched and partitioned steel analysed by atom probe tomography. In *Proceedings of the 3rd International Symposium on Steel Science, Kyoto, Japan, The Iron and Steel Institute of Japan, 27–30 May 2012*.
10. De Knijf, D.; Santofimia, M.J.; Shi, H.; Xu, W.; Föjer, C.; Petrov, R. In situ austenite–martensite interface mobility study during annealing. *Acta Mater.* **2015**, *90*, 161–168.
11. Seo, E.J.; Cho, L.; De Cooman, B.C. Kinetics of the partitioning carbon and substitutional alloying elements during quenching and partitioning (Q & P) processing of medium Mn steel. *Acta Mater.* **2016**, *107*, 354–365.
12. Ayenampudi, S.; Celada-Casero, C.; Sietsma, J.; Santofimia, M.J. Microstructure evolution during high-temperature partitioning of a medium-Mn quenching and partitioning steel. *Materialia* **2019**, *8*, 100492.
13. Gibbs, P.; De Moor, E.; Merwin, M.J.; Clausen, B.; Speer, J.G.; Matlock, D.K. Austenite stability effects of tensile behavior of manganese-enriched -austenite transformation-induced plasticity steel. *Metall. Mater. Trans. A* **2011**, *42*, 3691–3702.
14. Arlazarov, A.; Gouné, M.; Bouaziz, O.; Hazotte, A.; Petitgand, G.; Barges, P. Evolution of microstructure and mechanical properties of medium Mn steels during double annealing. *Mater. Sci. Eng. A* **2012**, *542*, 31–39.
15. Luo, H.; Shi, J.; Wang, C.; Cao, W.; Sun, X.; Dong, H. Experimental and numerical analysis on formation of stable austenite during the intercritical annealing of 5 Mn steel. *Acta Mater.* **2011**, *59*, 4002–4014.
16. Ding, R.; Dai, Z.; Huang, M.; Yang, Z.; Zhang, C.; Chen, H. Effect of pre-existed austenite on austenite reversion and mechanical behaviour of an Fe-0.2C-8Mn-2Al medium Mn steel. *Acta Mater.* **2018**, *147*, 59–69.
17. Santofimia, M.J.; Zhao, L.; Sietsma, J. Volume Change Associated to Carbon Partitioning from Martensite to Austenite. *Mater. Sci. Forum* **2012**, *706*, 2290–2295.

18. Kannan, R.; Wang, Y.; Li, L. Identification of Inverse Bainite in Fe-0.84C-1Cr-1Mn Hypereutectoid Low Alloy Steel. *Metall. Mater. Trans. A* **2017**, *48*, 948–952.
19. Onink, M.; Brakman, C.M.; Tichelaar, F.D.; Mittemeijer, E.J.; Van der Zwaag, S. The lattice parameters of austenite and ferrite in Fe-C alloys as functions of carbon concentration and temperature. *Scr. Metall. Mater.* **1993**, *29*, 1011–1016.



© 2020 by the authors. Licensee MDPI, Basel, Switzerland. This article is an open access article distributed under the terms and conditions of the Creative Commons Attribution (CC BY) license (<http://creativecommons.org/licenses/by/4.0/>).